

FUNDAMENTAL FREQUENCY VARIATION ANALYSIS OF CABLE-STAYED BRIDGES WITH DAMAGE CAUSED BY SUDDEN INCIDENTS

Hu Dandan¹, Baozhen Yan²

- 1. School of Intelligent and Construction Engineering, Harbin University, No.109 Zhongxing Road, Harbin, Heilongjiang Province, China; Hardandan@163.com*
- 2. Heilongjiang Province Highway Bridge Survey Design Co. Ltd., No. 90 Qingbin Road, Harbin 150040, China*

Received: 07.12.2024

Received in revised form: 10.09.2025

Accepted: 27.03.2026

ABSTRACT

Cable-stayed bridges have become one of the fastest growing and most competitive bridge types in modern bridge engineering due to their large spanning capacity and novel structure. Rapid economic development has led to a gradual increase in the number of vehicles transporting flammable and explosive products, as well as an increase in the incidence of bridge fires. Cable-stayed cables are usually close to the carriageway, and a fire will inevitably cause varying degrees of harm to the cable-stayed cables of a bridge in the event of a fire, leading to significant economic losses. Dynamic performance of cable-stayed bridges after fire is investigated by different simulation analyses of fire-induced damage to the tension cables. Results show that different tie damage has different effects on the dynamic characteristics of the whole bridge, and the tie damage has the greatest effect on the vertical symmetric bending formation, and almost no effect on the longitudinal drift, transverse bending and torsion formations. Damage to the outer cables near the transition span and side spans has a large effect on the low-order frequency variation of cable-stayed bridges, especially when the damage to the outermost back cables of S13+N13 occurs, it has the largest effect on the 2nd and 3rd order frequency variation, with a maximum value of 9.6%. Different levels of damage to the tension cables affect the dynamic performance of the bridge in terms of quantitative changes, with the frequency of a certain order formation increasing as the level of damage increases. It is particularly important to quickly and accurately analyze and evaluate the mechanics of overfire cable-stayed bridges to provide an accurate basis for decision-making.

KEYWORDS

Cable-stayed bridges, Cable-stayed cables, Sudden incidents, Fire, Fundamental frequency variation

INTRODUCTION

In recent years, with the increase in the number of automobiles and the acceleration of bridge construction, the probability of fire in the process of bridge construction and operation has increased, and the hazards of fire for bridges have received more and more attention. Fires caused by vehicles account for the majority of bridge fires [1-4]. Cable-stayed cables are usually in close proximity to the travel lanes, and fires, when they occur, will inevitably cause varying degrees of harm to the cable-stayed cables of a bridge [5-8].

Vehicle fire is a fortuitous event, due to the type of vehicle at the time of the incident is different, so that when the fire occurs cable-stayed cables in the fire at different temperatures, resulting in cable-stayed cables with varying degrees of damage, mild impact to the cable-stayed cables outside the HDPE sheath, so that the sheath charred and melted, and the serious can lead to the entire cable-stayed cables fracture [9-12]. In recent years, scholars at home and abroad have carried out more researches on the fire resistance of prestressed concrete structures, but there are fewer researches on the damage of cable-stayed bridges under fire, among which there are even fewer analyses on the force effects of cable-stayed bridges after damage of the cables [13-15].

In August 2011, a tanker loaded with 24 tons of gasoline had a rear-end collision with another coal hauling truck at Caogou Bridge in Yulin City's YuYang District, severely damaging the tank, leaking a large amount of gasoline, and starting a fire [16]. In January 2013, an oil truck in the Anqiu section of National Highway 206, Qingyunhu Lake bridge accidentally hit the bridge abutment, resulting in the rupture of the tank, the tank 30 tons of 93 gasoline leakage, the formation of a fire, gasoline plus the wind, the fire burned for a whole day, causing serious damage to the bridge [17].

At present, there is a lack of research on cable damage, especially in the case of cable fire damage, the overall performance of the bridge is more prominent impact and evaluation. This paper takes the bridge fire accident as the engineering background, and it is especially important to study the dynamic performance of cable-stayed bridges after the fire through different simulation analyses of fire-induced damages of tie cables by using the damage theory and finite element theory, which provides an accurate basis for decision makers to make decisions.

ENGINEERING BACKGROUND

In 2011 the bridge had a traffic accident, the car on fire near the cable-stayed cables burned, the accident damaged cable-stayed cables a total of two, respectively, for the north bank upstream of the N13, upstream of the N12 two back of the cable-stayed cables, two cable-stayed cables PE protective materials partially burned, cable-stayed cables there are obvious traces of damage by the fire, the two cable-stayed cables all appear to be exposed steel wire, cable-stayed cables of high-strength steel wire did not find the protruding deformation, wire breakage phenomenon. Upstream N12 cable-stayed cables PE protective material burned length of 16.5 m, upstream N13 cable-stayed cables PE protective material burned length of 5 m, set aside the burnt material, revealing the cable-stayed cables steel wire, steel wire surface color has a certain degree of discoloration. The damage to the cable is shown in Figure 1.



Fig.1 - Fire diagram of two back cables on the downstream side of the north bank

Main bridge adopts double-tower and double-surface semi-floating system combined with cable-stayed bridges, and approach bridge adopts prestressed concrete continuous box girder structure length of the bridge is 1268.86 m, the main bridge is 696 m long, the approach bridge is 572.86 m long, the main bridge adopts the form of 44 m (transition span)+136 m (side span)+336 m (main span)+136 m (side span)+44 m (transition span) bridge span arrangement, the design load: automobile-super 20 level, trailer-120, four lanes in both directions. Four lanes in both directions. The overall arrangement of the whole bridge and the panoramic arrangement of the whole bridge, as shown in Figure 2.

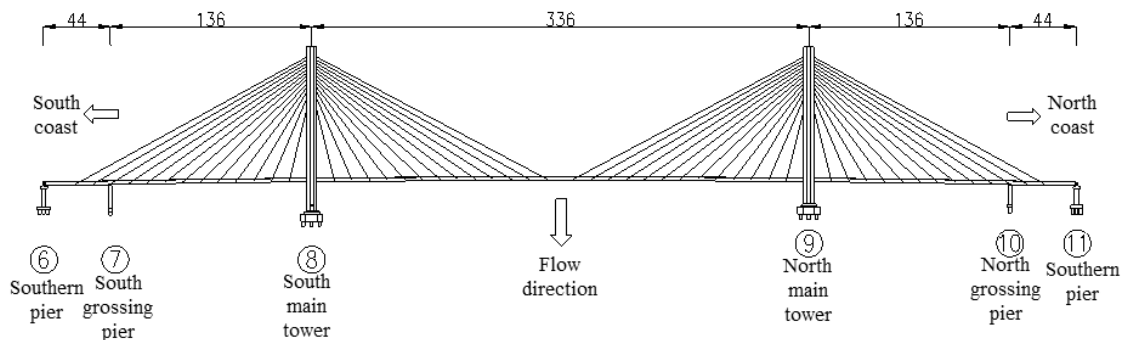


Fig.2 - Overall layout of the main bridge (unit: m)

(1) Bridge tower

Cable tower is a portal tower, set up the upper and lower beams. There is a lower crossbeam below the bridge deck and an upper crossbeam above the bridge deck, and the 2 crossbeams divide the bridge tower into three parts: the upper, middle and lower pylons. South tower is 110.80 m high, north tower is 106.10 m high, and the crossbeam of the tower is hollow box girder. Cross-sections of beams and tower columns are enlarged and strengthened with chamfers. A stiffening skeleton is provided in the wall of the tower. Inside the tower, there is a pedestrian ladder leading to the top of the tower. Pedestrian entrances are located at the top of the lower beam and the tower wall at the bridge deck.

(2) Main girder of the main bridge

Main girder section with two I-beam side beam ribs, cross girder and small longitudinal girder in the middle, combined with concrete deck slabs to form a combined section. Rib spacing of the two

I-beam side girders is 29.2 m. The girder height at the Bussel Road is 2.2 m, and the girder height at the centerline of the bridge is 2.47 m. The ratio of the girder height to the main span is 1/136, and the height-to-width ratio of the cross-section is 1/13.4.

(3) Cable-stayed cables

This bridge adopts hot-extruded polyethylene semi-parallel cable-stayed cables, and the cable-stayed cables are made of $\phi 7$ low relaxation prestressed galvanized high strength steel wire. Concentric and concentric twisting $2^{\circ}\sim 4^{\circ}$, outsourcing PE protective material. The total number of 52 pairs of cables in the bridge is 163~367 wires. The design cable strength is 3940 kN~8870 kN, and the layout of the cables on the north and south banks is shown in Figure 3.

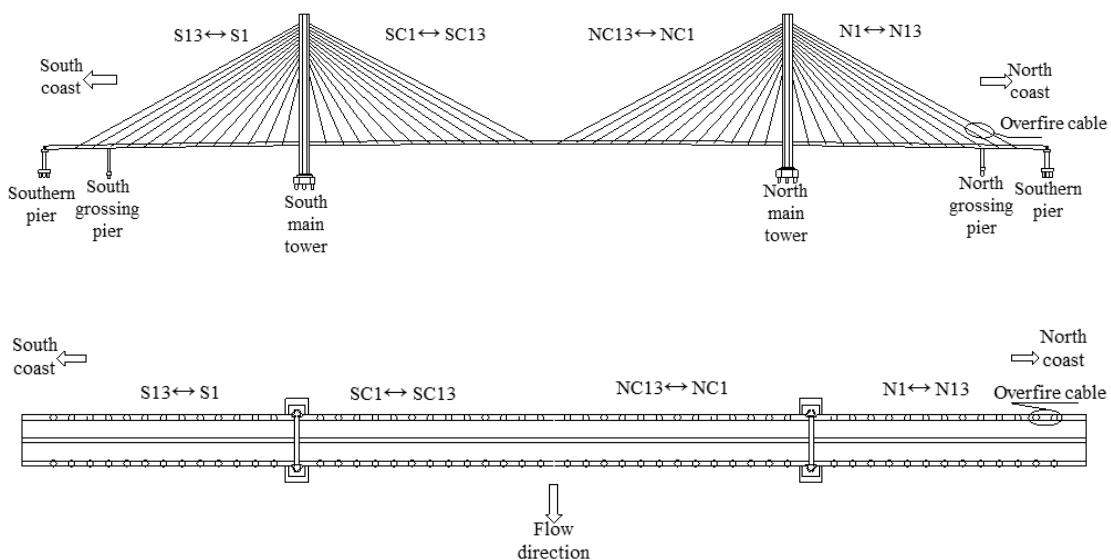


Fig.3 - Layout of cable on the north and south banks

DAMAGE MECHANISM of CABLE-STAYED CABLES

To study damage in structures, it is first necessary to choose the appropriate state parameter, damage variable, that characterizes the damage. Damage varies due to the diversity of substances. Differences in damage exogenous factors lead to different damage for the same substance [18-22].

Cable-stayed cables subjected to fire damage, according to the previous description of the damage mechanism of the cable-stayed cables for simulation, for the fire caused by high-strength steel wire bundle strand fracture, fracture of the steel wire part of the complete withdrawal from the work, for the fire did not melt off the steel wire, according to the occurrence of the temperature of the member of the overfire when the modulus of elasticity, ultimate strength calculations, the calculation of the specific method of calculation in combination with the previous high-temperature after the material characteristics of the steel for the calculations. Load carrying capacity of a cable is only related to the effective load bearing area of the cable \tilde{A} , and the study of cable damage is based on statistical theory. Take the entire high-strength steel wire bundle strand of the cable-stayed cables as a continuous medium, the ratio of the area of the fractured high-strength steel wire ($A - \tilde{A}$) to the area of the original high-strength steel wire of the cable-stayed cables is defined as the damage rate, as the damage variable D in the damage mechanism of the cable-stayed cables, then:

$$\zeta = (A - \tilde{A}) / A = 1 - \tilde{A} / A \quad (1)$$

After the damage to the material is assumed to break part of the steel wire for the second group of composite materials, according to the “law of mixing” of composite materials, after the damage to the cable-stayed cables of the modulus of elasticity, the ultimate strength of the cable-stayed cables for:

$$E_{\xi} = E(1 - \zeta) + E_K \zeta$$

$$\sigma_{\xi} = \sigma(1 - \zeta) + \sigma_K \zeta \quad (2)$$

Among them: ζ —Proportion of voids to the whole wire rope;

E —Modulus of elasticity of the non-destructive high-tensile steel wire;

E_K —Elastic modulus of the cavity;

σ_K —Limiting strength of the cavity.

Due to the elastic modulus of the cavity $E_K = 0$, the ultimate strength $\sigma_K = 0$ then:

$$E_{\xi} = E(1 - \zeta)$$

$$\sigma_{\xi} = \sigma(1 - \zeta) \quad (3)$$

For partially ablated cable-stayed cables the modulus of elasticity and ultimate strength shall be discounted in accordance with the above formula, and for cable-stayed cables affected by overfire the modulus of elasticity and ultimate strength of the steel wire after high temperatures shall be discounted in accordance with the degradation law of elasticity and ultimate strength of the steel wire after high temperatures as described in the preceding paragraphs.

Take a cable-stayed cables as an example, assuming that the cable-stayed cables are multiple parallel steel wire cable-stayed cables, and some of the steel wires are melted after the fire, and assuming that the cable-stayed cables have a damage rate ζ of 30%, then according to equation

$$(3) \quad E_{\xi} = E(1 - \zeta) = E(1 - 30\%) = 70\%E; \sigma_{\xi} = \sigma(1 - \zeta) = \sigma(1 - 30\%) = 70\%\sigma .$$

Assuming that the temperature of the high-tensile steel wire in the cable-stayed cables under the action of fire is 900 °C, and then according to the degradation model of elastic modulus and ultimate strength of the high-tensile steel wire after the fire, the modulus of elasticity and the ultimate strength of the cable-stayed cables after the fire will be reduced to 80.5% and 17.12% respectively of the original one, then the modulus of elasticity of the cable-stayed cables will be equivalent to $E^* = 70\%E80.5\% = 1.0988 \times 10^5 \text{ MPa}$, the limiting strength equivalent is $\sigma^* = 70\%\sigma80.5\% = 884 \text{ MPa}$

Therefore, the modulus of elasticity and ultimate strength of the cable-stayed cables after overfire are calculated as:

$$E_{\xi} = (1 - \zeta)E_{st}$$

$$\sigma_{\xi} = (1 - \zeta)\sigma_{st} \quad (4)$$

Among them: E_{ξ} —Modulus of elasticity of the whole cable after overfiring;

σ_{ξ} —Ultimate strength of the whole cable after overfiring;

ζ —Proportion of fused wire to the entire wire rope;

E_{st} —Modulus of elasticity of the unfused high-tensile steel wire in the cross-section of the cable after overheating at high temperature;

σ_{st} —Ultimate strength of the high-tensile steel wire after high temperature without fusing in the cross section of the cable after overheating.

FINITE ELEMENT ANALYSIS

Modeling

Finite element model of cable-stayed bridges was established by Midas/Civil. Main girder, small longitudinal beams, crossbeam: Both sides of the steel main girder ribs, small longitudinal beams and crossbeams are simulated by beam units, the steel main girder ribs are the main load-bearing members, which are connected with the middle small longitudinal beams through steel crossbeams to form a space girder lattice structure, the steel crossbeams are connected with the main girder and the small longitudinal beams through the common nodes. Concrete bridge deck slabs are simulated by means of a uniform force form, which is loaded on the main girder ribs, small longitudinal girders and cross girders connected to them. Bridge towers are modeled using beam units. Top and bottom beams are connected to the portal tower columns by shared nodes. The simulation of cable-stayed cables is carried out by using truss unit, the upper end of the cable establishes a node at the outer edge of the bridge tower, the lower end establishes a node at the outer edge of the steel main girder, and the two ends of the cable are connected with the bridge tower and the main girder by stiffening arms. A total of 1,933 nodes and 2,272 units are established for the whole bridge. A total of 104 cable-stayed cables are simulated by truss units, and the main tower and main girder, which are subject to bending pressure, are simulated by beam units. The damage to the cables in the text is achieved by reducing the elastic modulus of the stay cables. By adjusting the elastic modulus of the stay cables, the mechanical performance changes of the cables under different degrees of damage can be equivalently simulated. Structural finite element discretization diagram is shown in Figure 4.

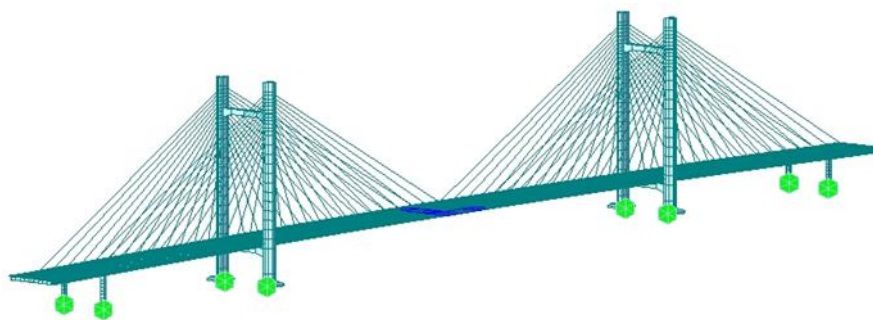


Fig.4 - Structural finite element discretization

DYNAMIC PERFORMANCE of CABLE-STAYED BRIDGES UNDER DAMAGE to CABLES

Analysis of Structural Dynamics Under Symmetric Fire-Induced Meltdown of Cables

S1+N1, S3+N3 are selected as two working conditions for the fused damage of cables at the tower root, S6+N6, S8+N8 are two working conditions for the fused damage of cables at the middle of the span, and S11+N11, S13+N13 are two working conditions for the fused damage of cables at the outer back cables, and in total, six conditions are selected for the comparative analysis of the impacts of the auxiliary spans and side spans of the cable power. Table 1 shows the frequency and formation results of different symmetrical fusion damage of cables in the main span. SC1+NC1 and SC3+NC3 are selected as two working conditions for the fusion damage of cables at the tower root of the main span, SC6+NC6 and SC8+NC8 are selected as two working conditions for the fusion damage of cables at the 1/4L of the main span, SC11+NC11 and SC13+NC13 are selected as two working conditions for the fusion damage of cables at the middle of the span, which is a total of 6 working conditions for the comparative analysis of the impact of main span cable dynamics. conditions for the comparative analysis of the dynamic impact of the main span cables.

Tab. 1 - Structural intrinsic frequencies and formations for different cable symmetric fire-induced fusion cases in the main span

Ordinal number	Non destructive model frequency	Formation	Ordinal number	Non destructive model frequency	Formation
1	0.127	Drifting vertically	11	1.133	Beam positive symmetrical vertical bending + tower positive symmetrical smooth bending
2	0.363	First-order symmetrical vertical bending of beams	12	1.219	Beam antisymmetric vertical bending + tower antisymmetric smooth bending
3	0.460	First-order antisymmetric vertical bending of beams	13	1.244	Beam positive symmetrical vertical bend
4	0.472	South tower first-order lateral bend	14	1.364	Beam opposes symmetrical vertical bend
5	0.488	North tower first-order lateral bend	15	1.447	Beam symmetric torsion + tower symmetric lateral bending
6	0.651	First-order symmetric transverse bending of beams	16	1.531	Beam positive symmetrical vertical bending + tower positive symmetrical smooth bending
7	0.733	Second-order symmetric vertical bending of beam + symmetric smooth bending of tower	17	1.566	Beam symmetric transverse bending + tower positive symmetric downward bending
8	0.839	Second-order antisymmetric vertical bending of beam + antisymmetric smooth bending of tower	18	1.606	Beam positive symmetrical vertical bending + tower positive symmetrical smooth bending
9	0.890	Positive symmetric vertical bending at beam height order	19	1.649	Beam antisymmetric torsion + tower antisymmetric side bending
10	1.003	Beam high-order antisymmetric vertical bending + tower antisymmetric smooth bending	20	1.687	Beam antisymmetric transverse bending + tower antisymmetric smooth bending

Figures 5 and 6 show the frequency-order plots and frequency-variation-order plots for the first 20 orders of various operating conditions for different cables fused at the transition span and side spans. It can be seen that the amount of change in frequency is very small, with the largest variation in the S13+N13 condition, where the maximum frequency variation is only 9.6%.

In order to facilitate the analysis of the frequency variation-order diagrams for different working conditions are listed separately, and Figures 7 to 9 show the frequency comparison diagrams for the transition span and inside side span, mid-span and outside working conditions, respectively.

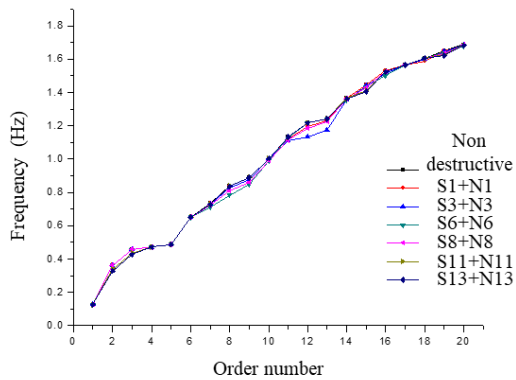


Fig.5 - Frequency-order variation under fire-induced meltdown of different cables in transition span and side spans

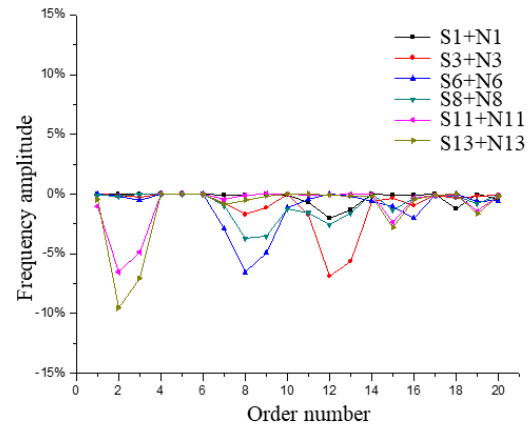


Fig.6 - Frequency variation-order variation plots under fire-induced fusing of different cables for transition and side spans

From Figures 7 to 9, it can be concluded that the transition span and side span cable damage has an effect on the vertical bending formation of the whole bridge and has the greatest effect on the vertical symmetric bending formation, and the damage of the cable near the outer side has the greatest frequency on the formation.

Damage to the outer cables near the transition span and side spans has a large effect on the low-order frequency variation of cable-stayed bridges, especially when the damage to the outermost back cables of S13+N13 occurs, it has the largest effect on the 2nd and 3rd order frequency variation, with a maximum value of 9.6%. Transition span and side span cable damage has almost no effect on the longitudinal drift, transverse bending and torsional formations of the cable-stayed bridges.

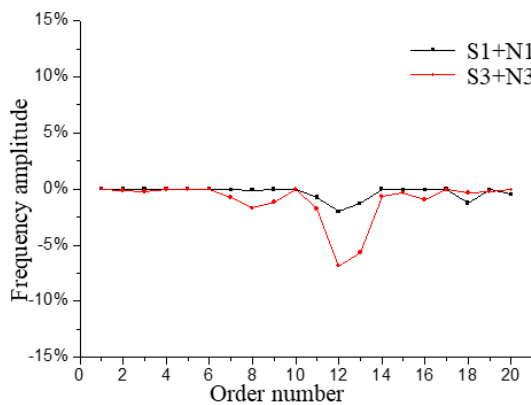


Fig.7 - Frequency amplitude order diagram of transition span and inner side span

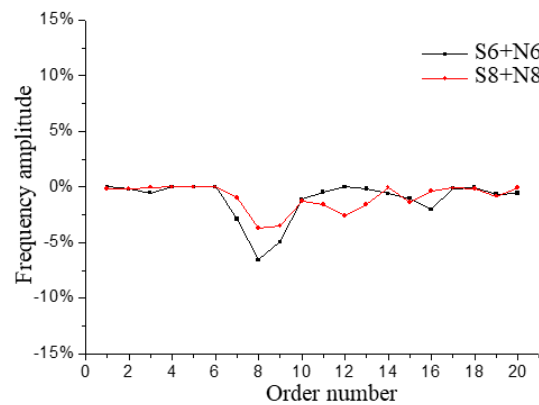


Fig.8 - Frequency amplitude order diagram of transition span and edge span

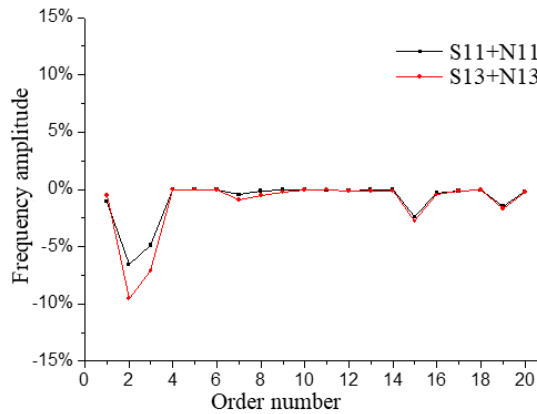


Fig.9 - Transition span and side span outer frequency variation-order plot

Figures 10 and 11 show the frequency-order and frequency variation-order plots for the first 20 orders of various working conditions for different cables fused on the main span. It can be seen that the amount of frequency change is very small, the SC13+NC13 condition has the largest variation, and the maximum frequency variation is only 11.1%.

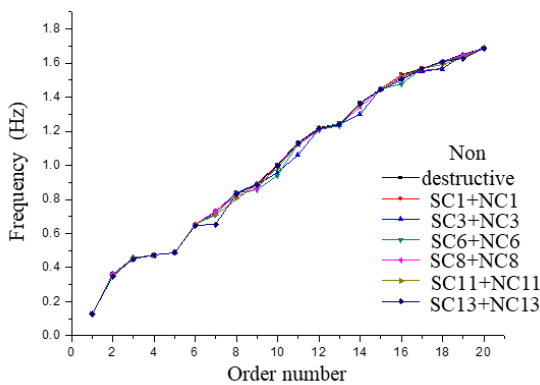


Fig.10 - Frequency-order variation under different cable fusing in main span

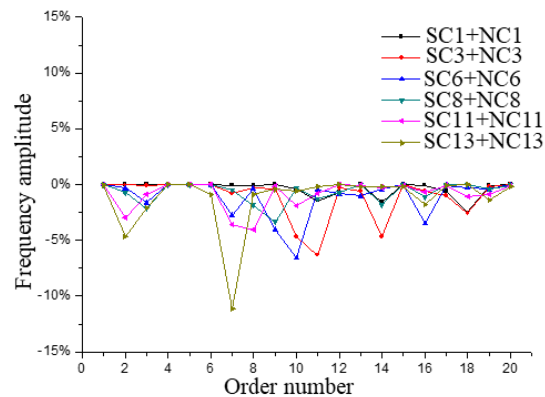


Fig.11 - Plot of frequency variation-order change under fire-induced fusing of different cables in the main span

In order to facilitate the analysis of the frequency amplitude-order plots for different conditions are listed separately. Figures 12 to 14 show the comparison of the frequency amplitude for the main span near the bridge tower, 1/4L and mid-span damage conditions, respectively.

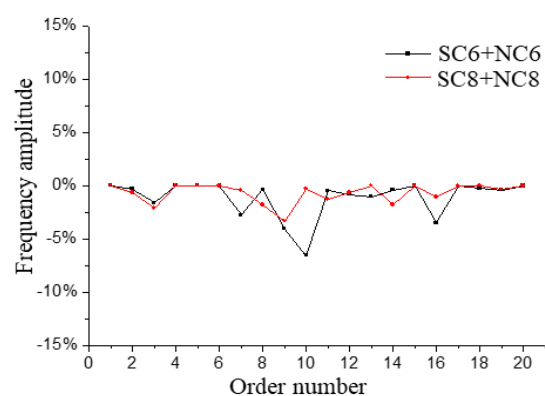
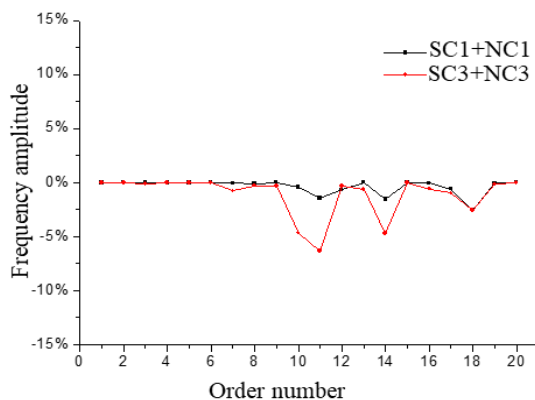


Fig.12 - Frequency variation-order plot of the main span near the side of the bridge tower

Fig.13 - Frequency variation-order plot at 1/4L of main span

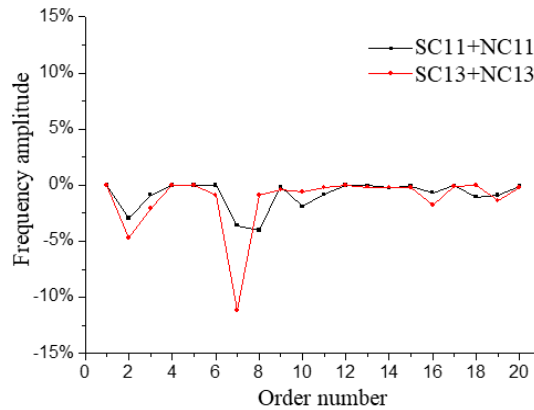


Fig.14 - Main span mid-span frequency variation-order plot

From Figures 12 to 14, it can be seen that the main span cable damage has an effect on all vertical bending formations of the whole bridge, with the greatest effect on the vertical symmetric bending formations, and the damage close to the outer cables has the greatest effect on the frequency of the formations. The mid-span cable has a large effect on the low-order frequency, and near the bridge tower has a large effect on the high-order frequency.

Damage to the cable near the mid-span of the main span has a large effect on the lower order frequencies of the cable-stayed bridges, especially when the damage to the outermost back cables of SC13+NC13 occurs, it has the largest effect on the 7th order frequencies, with a maximum value of 11.1%. Transition span and side span cable damage has almost no effect on the transverse bending and torsional formations of the cable-stayed bridges structure.

Structural Dynamic Analysis of The Whole Bridge Under Different Cable Fire Damage

Analysis of Structural Dynamics Under Asymmetric Fire-Induced Fusing of Cables

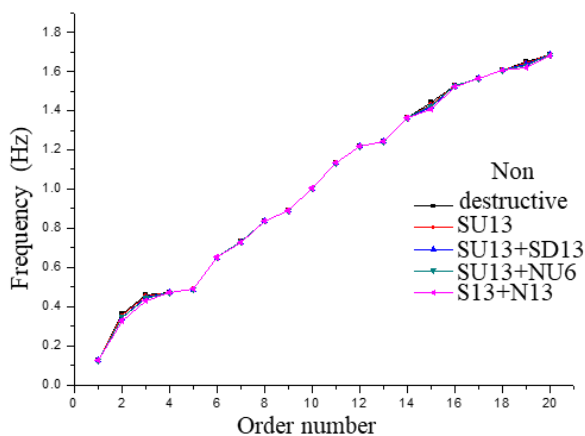


Fig.15 - Frequency-order diagram under asymmetric damage of transition span and side span

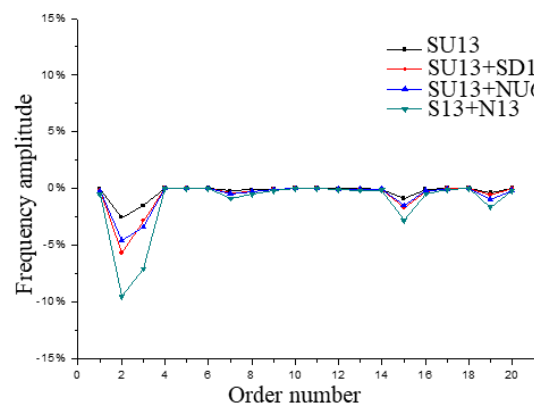


Fig.16 - Frequency variation-order plot under asymmetric damage of transition span and side span

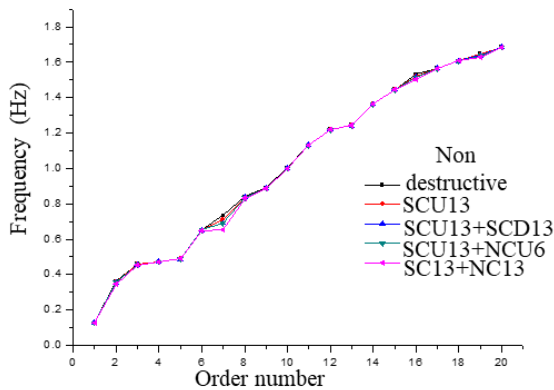


Fig. 17 - Frequency-order diagram under asymmetric damage in the main span

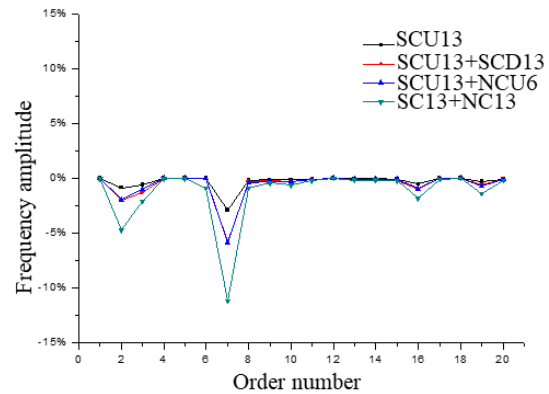


Fig. 18 - Frequency variation-order plot under asymmetric damage of main span

From the previous section, it is concluded that the long cable fusion has the greatest effect on the lower order frequencies, so the transition span and side span outermost back cables are used to represent the auxiliary and side span cable asymmetric damage, and the main span outermost back cable is used to represent the main span cable asymmetric damage. Table 3-13 shows the first 20 orders of frequency values for the transition span, side span cable asymmetry and main span cable asymmetry damage cases, which are analyzed by taking four working conditions (both asymmetric span and asymmetric axis, symmetric longitudinal axis but asymmetric span, symmetric span but asymmetric longitudinal axis, and both symmetric span and symmetric longitudinal axis), respectively.

Figures 15 and 16 show the frequency-order and frequency-variation-order plots under asymmetric fusing damage in the transition span and side spans, as shown in the two figures:

Transition span and side span asymmetric damage had a large effect on the frequency of 2nd and 3rd order vertical bending formations (first order vertical symmetric and antisymmetric formations), and on the frequency of 15th and 19th order torsional formations (positive symmetric torsion and antisymmetric torsion), which increased with the increase in the number of fused cables, and had almost no effect on the frequency of the other side bending formations.

Figures 17 and 18 show the frequency-order and frequency-variation-order plots under the main-span asymmetric fusion damage. It can be seen from the two plots that the main-span asymmetric damage has a greater effect on the frequency of the vertical bending formations, with the maximum effect being on the 2nd and 7th orders, and has a greater effect on the frequency of the 19th-order torsional formations (antisymmetric torsion), and with the increase in the extent of the damage, the formation frequency variation increases, and has almost no effect on the frequency of other lateral bending

Structural Dynamic Analysis of The Whole Bridge with Different Degrees of Fire Damage to The Cables

In order to analyze the structural dynamic characteristics of the whole bridge under different degrees of fire damage, two pairs of back cables and their adjacent cables are selected for the analysis of the dynamic characteristics under different degrees of damage, S13 and S12 are taken to represent different degrees of damage in the transition span and side spans at the same time, and SC13 and SC12 are taken to represent different degrees of damage in the main span at the

same time. Table 3-14 shows the values of the first 20 orders of formation frequency for the whole bridge structure at different damage levels of auxiliary and side spans and different damage levels of main spans.

Figures 19 and 20 show the frequency-order and frequency-variation-order plots of the structural formations at different levels of damage in the transition span and side spans.

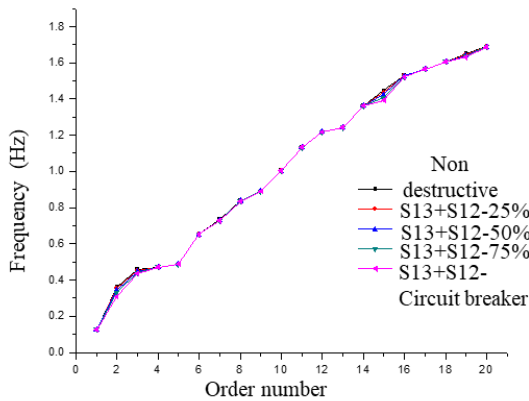


Fig. 19 - Frequency-order diagrams for different degrees of damage in the transition span and side spans

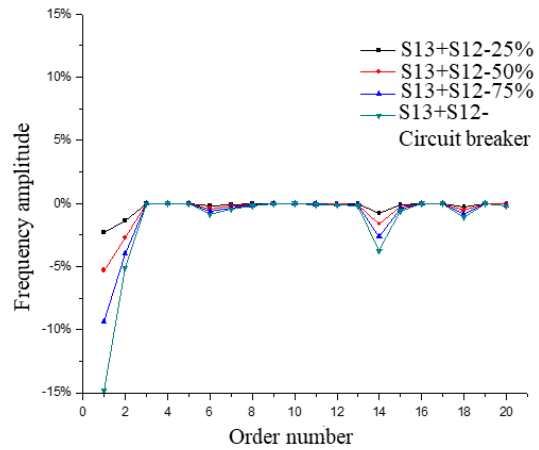


Fig. 20 - Frequency variation-order plots for different degrees of damage in the transition span and side spans

As can be seen from Figures 19 and 20, the effect on the frequency of the longitudinal floating formation (1st order) is larger for different damage levels of the transition span and side spans, and the effect on the bending formation of the antisymmetric vertical bending (2nd and 14th order) is larger, and the change in the frequency of the formations is larger with the increase of the damage level. There is almost no effect on the transverse bending and twisting formations.

Figures 21 and 22 show the frequency-order and frequency-variation-order plots for structural formations with different degrees of damage to the main span.

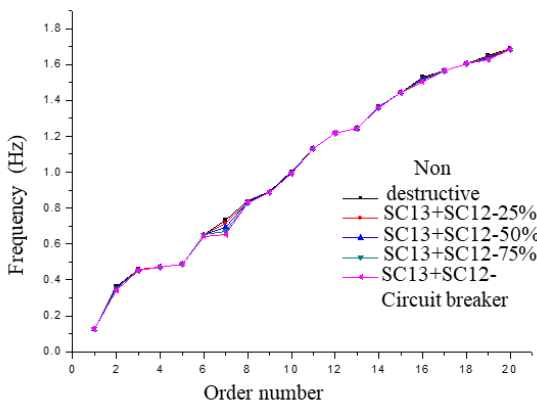


Fig. 21 - Frequency-order diagrams for different degrees of damage to the main span

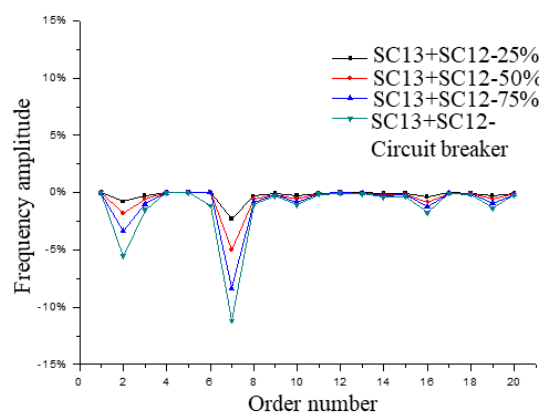


Fig. 22 - Frequency variation-order plot for different degrees of damage to the main span

From Figures 21 and 22, it can be seen that different degrees of damage to the main span

cables have a greater effect on the vertical antisymmetric bending formations (2nd and 7th order) of the structure, and the change in the frequency of the structural formations increases with the increase in the degree of damage. There is almost no effect on the longitudinal drift, transverse bending and torsion formations.

CONCLUSION

In this paper, the dynamic characteristics of the entire bridge under different cable fires and different degrees of cable fire damage were analyzed. The research results can provide references for the assessment of cable-stayed bridge damage, and also offer valuable insights for design. The main conclusions are as follows:

1. Fire-induced damage to the cables has an effect on the vertical bending formation of the whole bridge, with the greatest effect on the vertical symmetrical bending formation. Fire-induced damage to the whole bridge cables had little effect on the longitudinal drift, transverse bending and torsional formations of the cable-stayed bridges structure. Effects of different levels of damage to the cables on the dynamic performance of the bridge are reflected in quantitative changes, with the frequency of a certain order formation increasing as the level of damage increases.
2. At different levels of damage in the transition and side spans, the effect on the frequency of the longitudinal drift formation (1st order) is greater, and on the antisymmetric vertical bending (2nd and 14th order) bending formations, and the change in the frequency of the formations is greater with the increase in the level of damage. There is almost no effect on the transverse bending and twisting formations.
3. Damage to the outer cables near the transition span and side spans has a large effect on the low-order frequency variation of cable-stayed bridges, especially when the damage to the outermost back cables of S13+N13 occurs, it has the largest effect on the 2nd and 3rd order frequency variation, with a maximum value of 9.6%
4. The amplitude of frequency variation under the damage of the middle span cable is very small, while in the case of SC13 + NC13, the variation amplitude is the largest, with the maximum frequency variation being only 11.1%.

REFERENCE:

- [1] Zhang S, Shen R, Dai K, et al. A methodology for cable damage identification based on wave decomposition [J]. *Journal of Sound and Vibration*, 2019, 442: 527-551. <https://doi.org/10.1016/j.jsv.2018.11.018>
- [2] Hua X G, Ni Y Q, Chen Z Q, et al. Structural damage detection of cable-stayed bridges using changes in cable forces and model updating [J]. *Journal of structural engineering*, 2009, 135(9): 1093-1106. [https://doi.org/10.1061/\(ASCE\)0733-9445\(2009\)135:9\(1093\)](https://doi.org/10.1061/(ASCE)0733-9445(2009)135:9(1093))
- [3] Tang Z F, Sui X D, Duan Y F, et al. Guided wave-based cable damage detection using wave energy transmission and reflection[J]. *Structural Control and Health Monitoring*, 2021, 28(5): e2688. <https://doi.org/10.1002/stc.2688>
- [4] Kotsovinos P, Judge R, Walker G, et al. Fire performance of structural cables: Current understanding, knowledge gaps, and proposed research agenda [J]. *Journal of Structural Engineering*, 2020, 146(8): 03120002. [https://doi.org/10.1061/\(ASCE\)ST.1943-541X.0002703](https://doi.org/10.1061/(ASCE)ST.1943-541X.0002703)

- [5] Zhao S, Li G, Wang C. Bridge cable damage identification based on acoustic emission technology: A comprehensive review [J]. *Measurement*, 2024, 115: 115195. <https://doi.org/10.1016/j.measurement.2024.115195>
- [6] Iordachescu M, Valiente A, De Abreu M. Damage tolerance and failure analysis of tie-down cables after long service life in a cable-stayed bridge [J]. *Engineering Failure Analysis*, 2021, 125: 105437. <https://doi.org/10.1016/j.engfailanal.2021.105437>
- [7] Feng J, Gao K, Gao W, et al. Machine learning-based bridge cable damage detection under stochastic effects of corrosion and fire [J]. *Engineering Structures*, 2022, 264: 114421. <https://doi.org/10.1016/j.engstruct.2022.114421>
- [8] Baltazar A, Hernandez-Salazar C D, Manzanares-Martinez B. Study of wave propagation in a multiwire cable to determine structural damage [J]. *Ndt & E International*, 2010, 43(8): 726-732. <https://doi.org/10.1016/j.ndteint.2010.08.007>
- [9] Ren J, Zhang B, Zhu X, et al. Damaged cable identification in cable-stayed bridge from bridge deck strain measurements using support vector machine [J]. *Advances in Structural Engineering*, 2022, 25(4): 754-771.
- [10] Lin S W, Yi T H, Li H N, et al. Damage detection in the cable structures of a bridge using the virtual distortion method [J]. *Journal of Bridge Engineering*, 2017, 22(8): 04017039. [https://doi.org/10.1061/\(ASCE\)BE.1943-5592.0001072](https://doi.org/10.1061/(ASCE)BE.1943-5592.0001072)
- [11] Kildashti K, Alamdari M M, Kim C W, et al. Drive-by-bridge inspection for damage identification in a cable-stayed bridge: Numerical investigations [J]. *Engineering structures*, 2020, 223: 110891. <https://doi.org/10.1016/j.engstruct.2020.110891>
- [12] Yan B, Wang Y. Cable-stayed bridge Static performance with different cable damage condition caused by fire [J]. *Civil Engineering Journal*, 2025, 34(3). <https://doi.org/10.14311/CEJ.2025.03.0027>
- [13] Yang L, Shi G, Yin H, et al. Full-scale experimental study on the influence of damages on the static behavior of the single-layer cable net structure [C]// *Structures*. Elsevier, 2015, 3: 153-162. <https://doi.org/10.1016/j.istruc.2015.04.002>
- [14] Wang G, Ye J. Localization and quantification of partial cable damage in the long-span cable-stayed bridge using the abnormal variation of temperature-induced girder deflection [J]. *Structural Control and Health Monitoring*, 2019, 26(1): e2281. <https://doi.org/10.1002/stc.2281>
- [15] Bennetts I, Moinuddin K. Evaluation of the impact of potential fire scenarios on structural elements of a cable-stayed bridge [J]. *Journal of Fire Protection Engineering*, 2009, 19(2): 85-106.
- [16] Yang W, Huang J, Wang P, et al. An intelligent distributed sensor developed for power cable external damage monitoring [J]. *Procedia Computer Science*, 2021, 183: 166-174. <https://doi.org/10.1016/j.procs.2021.02.046>
- [17] Wu G M, Yi T H, Yang D H, et al. Damage identification of tie-down cables in cable-stayed bridges using vehicle-induced displacement [J]. *Journal of Performance of Constructed Facilities*, 2021, 35(3): 04021011. [https://doi.org/10.1061/\(ASCE\)CF.1943-5509.0001590](https://doi.org/10.1061/(ASCE)CF.1943-5509.0001590)
- [18] An Y, Zhong Y, Tan Y, et al. Experimental and numerical studies on a test method for damage diagnosis of stay cables [J]. *Advances in Structural Engineering*, 2017, 20(2): 245-256.
- [19] Lonetti P, Pascuzzo A. Vulnerability and failure analysis of hybrid cable-stayed suspension bridges subjected to damage mechanisms [J]. *Engineering Failure Analysis*, 2014, 45: 470-495. <https://doi.org/10.1016/j.engfailanal.2014.07.002>
- [20] Serra S, Montanari G C, Mazzanti G. Theory of inception mechanism and growth of defect-induced damage in polyethylene cable insulation [J]. *Journal of applied physics*, 2005, 98(3). <https://doi.org/10.1063/1.1978986>
- [21] Gao Q, Duan M, Liu X, et al. Damage assessment for submarine photoelectric composite cable under anchor impact [J]. *Applied Ocean Research*, 2018, 73: 42-58. <https://doi.org/10.1016/j.apor.2018.01.006>
- [22] Hao H, Tang E K C. Numerical simulation of a cable-stayed bridge response to blast loads, Part II: Damage prediction and FRP strengthening [J]. *Engineering Structures*, 2010, 32(10): 3193-3205. <https://doi.org/10.1016/j.engstruct.2010.06.007>